

Absolute Quantification of Nanoparticle Interactions with Individual Human B Cells by Single Cell Mass Spectrometry

Nathan D. Donahue, Vinit Sheth, Alex N. Frickenstein, Alyssa Holden, Sandy Kanapilly, Chady Stephan, and Stefan Wilhelm*



Cite This: <https://doi.org/10.1021/acs.nanolett.2c01037>



Read Online

ACCESS |



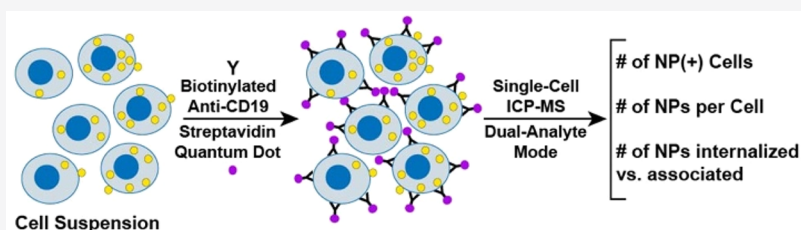
Metrics & More



Article Recommendations



Supporting Information



ABSTRACT: We report on the absolute quantification of nanoparticle interactions with individual human B cells using quadrupole-based inductively coupled plasma mass spectrometry (ICP-MS). This method enables the quantification of nanoparticle–cell interactions at single nanoparticle and single cell levels. We demonstrate the efficient and accurate detection of individually suspended B cells and found an ~ 100 -fold higher association of colloiddally stable positively charged nanoparticles with single B cells than neutrally charged nanoparticles. We confirmed that these nanoparticles were internalized by individual B cells and determined that the internalization occurred via energy-dependent pathways consistent with endocytosis. Using dual analyte ICP-MS, we determined that $>80\%$ of single B cells were positive for nanoparticles. Our study demonstrates an ICP-MS workflow for the absolute quantification of nanoparticle–cell interactions with single cell and single nanoparticle resolution. This unique workflow could inform the rational design of various nanomaterials for controlling cellular interactions, including immune cell–nanoparticle interactions.

KEYWORDS: Nanoparticle, B cell, Nano-Bio Interactions, Single-Cell ICP-MS, Elemental Analysis, Mass Spectrometry

Engineered nanoparticles can deliver antigens and nucleic acid based payloads for immune system activation to induce safe and durable immune responses.^{1–3} This activation process often includes B cells that mediate antibody-dependent responses and assist with long-lasting immunity.^{4–6} Nanoparticles may interact with B cells in organs and tissues, such as the liver, spleen, and lymph nodes, impacting nanoparticle delivery efficiency, activity, fate, and toxicity.^{7–12} To develop safe and effective nanoparticle formulations for immune system activation, there is a need to quantify the interactions between nanoparticles and immune cells, such as individual B cells, at the single cell level.

Typically, flow cytometry provides single cell analysis of nanoparticle–cell interactions. However, in flow cytometry, nanoparticles may require fluorophores that can alter a nanoparticle’s physicochemical properties, therefore often affecting cellular association and uptake.^{13,14} Fluorophore-free measurements with flow cytometry using light scattering of cells exposed to nanoparticles have been performed but rely on nanoparticles >20 nm in size (Table S1).^{15–17} Similarly, microscopy-based analyses of nanoparticle–cell interactions are often limited by fluorescence and typically exhibit low-throughput (Table S1).^{18,19}

By contrast, mass spectrometry methods (e.g., CyTOF) have been applied to examine nanoparticle–cell interactions at the single cell level with multielement capabilities used for deep phenotyping of diverse cell populations (Table S1).^{20–22} As an economical alternative to these existing techniques, quadrupole-based inductively coupled plasma mass spectrometry (ICP-MS) is a promising method for quantifying nanoscale interactions.²³ Researchers have used single cell ICP-MS (SC-ICP-MS) to probe nanoparticle interactions with algae, yeast, and bacteria.^{24–27} Other studies using SC-ICP-MS investigated intrinsic metals, metallodrugs, and nanoparticles within various human cell lines.^{28–31} In this report, we demonstrated that quadrupole SC-ICP-MS detected metal-tagged human B cells at a rate of ~ 30 cells per second with a 50% transport efficiency. We quantified model gold nanoparticles (AuNPs)

Received: March 14, 2022

Revised: April 27, 2022

within single B cells and further demonstrated that >80% of B cells had internalized AuNPs.

We first sought to compare two different cell labeling methods to count individual B cells with SC-ICP-MS accurately. The first method relied on an iridium-based DNA intercalator, commonly used in mass cytometry to nonspecifically mark nucleated single cells (Figure 1A).³² The second cell

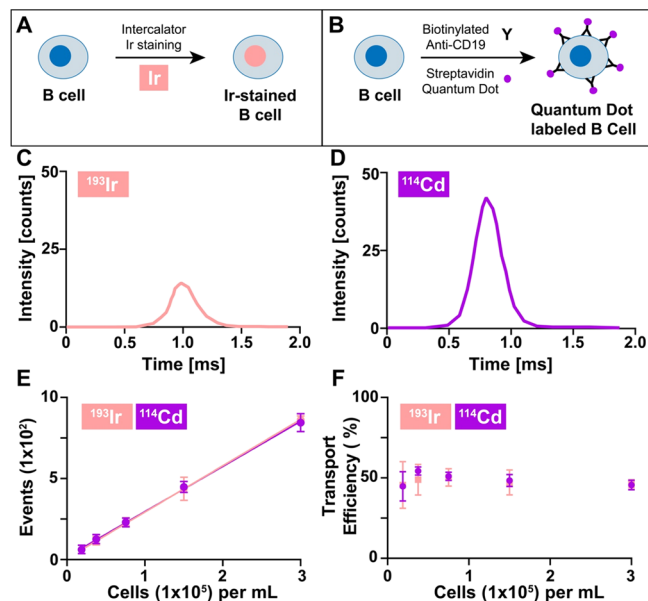


Figure 1. Detection of individual metal-labeled B cells. (A) Schematic representation of nucleic acid intercalator staining with natural-abundance iridium of individual B cells. (B) Schematic representation of labeling individual B cells with cadmium-based streptavidin-conjugated quantum dots via biotinylated anti-CD19 antibodies. (C) Transient ¹⁹³Ir ion signal of individual iridium-stained B cells. (D) Transient ¹¹⁴Cd ion signal of individual cadmium-based quantum dot labeled B cells. (E) Detected cell events as a function of cell concentration for ¹¹⁴Cd ($r^2 = 0.99$) and ¹⁹³Ir ($r^2 = 0.99$). Symbols represent averages and standard deviations of 3 independent experiments. Scan time = 30 s. (F) Transport efficiencies of individual B cells based on detected events from (E) and calculated using eq S1. Symbols represent averages and standard deviations of three independent experiments. The total acquisition scan time was 30 s for each measurement.

labeling method used streptavidin-coated quantum dots that selectively bound to specific biotin-conjugated antihuman CD19 monoclonal antibodies (Figure 1B). We hypothesized that, in contrast to the iridium staining, quantum dot labeling of B cells would generate a stronger ion signal per cell once the cells were atomized and ionized by the argon-based ICP (Table S2, Figure S1). To test this hypothesis, we prepared a single cell suspension of B cells that were stained with the iridium intercalator (Figure 1A). Additionally, we prepared B cells labeled with commercially available 15 nm streptavidin-coated Cd-based quantum dots consisting of a CdSe core and a ZnS shell and exhibiting an emission maximum of ~655 nm (Figure S2). To label B cells with streptavidin-modified quantum dots, we leveraged the ubiquitous surface expression of CD19.^{33,34} First, we incubated B cells with biotinylated antihuman CD19 monoclonal antibodies and then used streptavidin-coated Cd-based quantum dots to selectively bind to the biotinylated B cells (Figure 1B).^{35,36} To confirm the specific binding properties of streptavidin-coated quantum

dots to biotinylated antibodies, we prepared mixtures of quantum dots with and without biotinylated anti-CD19 antibodies and quantified the corresponding ¹¹⁴Cd signals using single particle ICP-MS (SP-ICP-MS) following previous SP-ICP-MS techniques.^{23,37} Using SP-ICP-MS, we observed a 5-fold enhancement of ¹¹⁴Cd intensity for streptavidin quantum dots mixed with biotinylated anti-CD19 antibodies when compared to quantum dots alone (Figure S3). These SP-ICP-MS results indicated successful clustering of streptavidin-coated quantum dots with biotinylated anti-CD19 antibodies. Additionally, we used fluorescence-based confocal laser scanning microscopy (CLSM) to confirm the surface labeling of B cells with the fluorescent quantum dots in the presence of antihuman CD19 monoclonal antibodies (Figure S4).

We then quantified the corresponding transient ion signals of individual iridium- and quantum dot-labeled B cells, respectively (Figure 1C,D). Iridium-stained B cells produced transient ¹⁹³Ir signals with ~15 counts (Figure 1C), while quantum dot labeled B cells produced transient ¹¹⁴Cd signals with ~42 counts (Figure 1D). These transient ion signals and corresponding counts indicated that quantum dot labeling of B cells enhanced the ion signal of individual B cells ~3-fold. These observations were consistent with the expected larger number of ions obtained from a single B cell labeled with 15 nm Cd-based quantum dots compared to the iridium staining. Our demonstrated quantum-dot-based labeling of individual cells in combination with biotinylated antibodies that recognize specific cell surface markers represents a potentially generalizable method to identify a particular type of cell for a given heterogeneous biological sample to analyze nanoparticle–cell interactions using the described quadrupole-based SC-ICP-MS workflow.

We then sought to confirm that intact and individual B cells entered the ICP-MS (Figure S1). To confirm this, we sequentially measured ¹¹⁴Cd and ¹⁹³Ir events with SC-ICP-MS at various B cell concentrations obtained from a suspension of single B cells. Figures S5 and S6 show the hemocytometer images of B cells obtained from stock single cell suspensions. We observed that both ¹¹⁴Cd and ¹⁹³Ir provided similar detected events at equivalent cell concentrations using SC-ICP-MS (Figure 1E). Next, we confirmed that these detected events corresponded to single intact B cells with epifluorescence microscopy. Figure S7 confirms that B cells remained intact upon nebulization and entry into the ICP-MS. Image analysis corroborated these findings and revealed Pearson correlation values of 0.9 pre- and post-nebulization for the B cell membranes and nuclei. Taken together, these results indicate that intact B cells entered the ICP-MS and were accurately detected with single cell resolution using SC-ICP-MS.

Based on the ¹¹⁴Cd and ¹⁹³Ir events in Figure 1E, we calculated the cellular transport efficiency using equation S1 (Figure 1F). The cellular transport efficiency enabled us to determine how many cells were detected upon entry into the ICP-MS, which we then applied to quantify the mass of various isotopes in individual B cells.³⁸ Using Equation S1, we found that the B cell transport efficiency was ~50% for both iridium staining and quantum dot labeling procedures at all cell concentrations used. Our results are significant since typical transport efficiencies for SC-ICP-MS are between 1% and 5%, with a throughput lower than ten cells per second.^{39–41}

We validated these results with commercially available micron-sized lanthanide-doped polymer beads as a model

system for single cells.^{24,42} At similar concentrations as the B cells, single lanthanide-doped beads were detected at a rate of ~ 40 events per second, yielding a transport efficiency of $\sim 60\%$ (Figure S8), representing the upper limit for this technique. We emphasize that with (i) microsecond detector dwell times, (ii) sample flow rates of $13.0 \mu\text{L}/\text{min}$, (iii) cell concentrations $\leq 3 \times 10^5$ cells/mL, (iv) 50% transport efficiency, and (v) single cell suspensions with intact B cells (Figures S5, S6, and S7), the probability of measuring overlapping/multiple cell events was minimized below a probability of 0.05 per Poisson statistics.⁴³ Collectively, these results confirmed consistent detection of intracellular and surface-bound metals on single and intact B cells with SC-ICP-MS. Based on these results, we then sought to quantify nanoparticle interactions at the single B cell level.

To model nanoparticle interactions with single B cells, we synthesized 13 nm quasi-spherical AuNPs with a narrow size distribution and tunable surface chemistry.⁴⁴ Using our previously established SP-ICP-MS method, we determined that 93% of the in-house synthesized AuNPs had a mass of ~ 24 ag, corresponding to an AuNP diameter of ~ 13 nm assuming a spherical geometry (Figure S9).³⁷ Transmission electron microscopy and dynamic light scattering measurements corroborated these SP-ICP-MS findings (Figure S10 and Table S3).

To probe how nanoparticle surface charge impacted interactions with individual B cells, we prepared 13 nm AuNPs with two different surface modifications according to previously published protocols: (i) neutral methoxy-terminated poly(ethylene glycol), mPEG, (1 kDa), or (ii) positively charged peptide (K7C) with a similar molecular weight as the 1 kDa mPEG.⁴⁵ These surface modifications yielded 13 nm AuNPs with similar hydrodynamic diameters but with a zeta potential difference of ~ 18 mV (Table S3). These nanoparticles with two different surface charges provided model systems to probe nanoparticle interactions with B cells. To ensure that the surface modifications did not compromise nanoparticle colloidal stability, we measured the mass of individual surface-modified 13 nm AuNPs under conventional cell culture conditions at 37°C . Our SP-ICP-MS data showed that the most frequent and average masses for both surface-modified AuNPs remained at ~ 24 ag, which indicated that the surface modifications did not result in detectable nanoparticle agglomeration (or aggregation) (Figure S11).³⁷

We hypothesized that positively charged AuNPs modified with K7C peptides containing seven lysine residues would associate more strongly with individual B cells than AuNPs modified with neutral mPEG potentially due to favorable electrostatic interactions with the overall negatively charged cell membrane.⁴⁶ We used SC-ICP-MS to quantify the average amount of ^{197}Au associated per individual B cell upon exposure to the differently charged 13 nm AuNPs under the same exposure conditions (Figure 2A). For B cells exposed to mPEG-modified AuNPs, the average ^{197}Au mass per cell was 315 ag, corresponding to ~ 13 AuNPs per cell. Conversely, B cells treated with the same molar concentration of K7C peptide-modified 13 nm AuNPs exhibited an average ^{197}Au mass of 30 117 ag per cell, corresponding to ~ 1250 AuNPs per cell. These results showed that peptide-modified AuNPs were nearly 2 orders of magnitude more effective in associating with individual B cells than the neutral mPEG-modified AuNPs. We then obtained the single cell ^{197}Au mass distribution of B cells exposed to either 13 nm mPEG-modified AuNPs or 13 nm

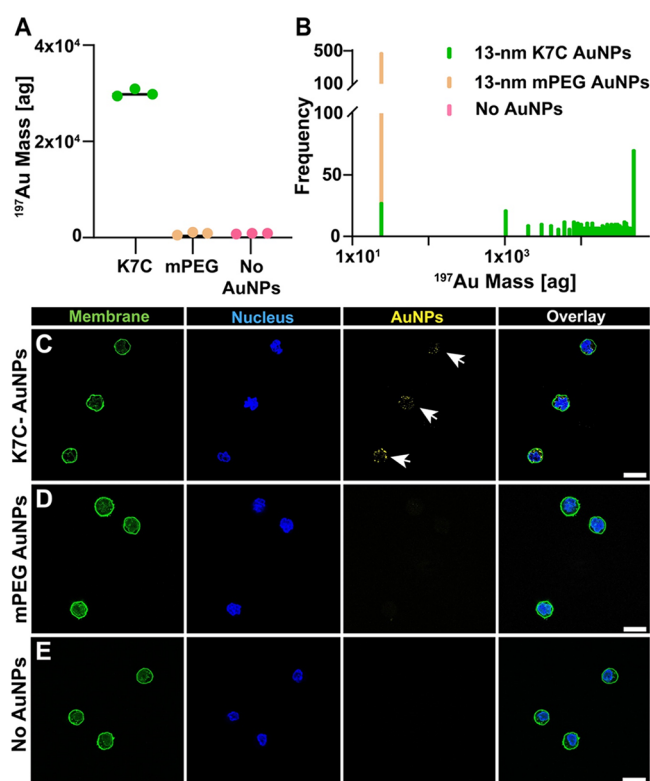


Figure 2. Quantifying and visualizing nanoparticle–cell association at the single-cell level. (A) The Average ^{197}Au masses obtained from B cells exposed to 13 nm K7C AuNPs, 13 nm mPEG AuNPs, or no AuNPs for 12 h. Circles represent the average ^{197}Au mass of ≥ 500 ^{197}Au events. Bars represent the average of 3 independent measurements. (B) Mass distribution of B cells exposed to either 13 nm K7C conjugated AuNPs (green), 13 nm mPEG conjugated AuNPs (orange), or no AuNPs (pink) for 12 h. Confocal laser scanning microscopy images of B cells exposed for 12 h to 13 nm K7C-modified AuNPs (C), 13 nm mPEG-modified AuNPs (D), and without AuNPs (E). Scale bars represent $20 \mu\text{m}$. The white arrows in (C) indicate the location of AuNPs.

K7C-modified AuNPs (Figure 2B). Interestingly, the most frequent mass of B cells exposed to mPEG-modified AuNPs was ~ 24 ag, the same mass of a single 13 nm AuNP (Figures S9 and S11). Only 4% of the total ^{197}Au events were above 24 ag for B cells exposed to 13 nm mPEG-modified AuNPs with a maximum detected mass of 13 000 ag per cell. On the other hand, $\sim 95\%$ of ^{197}Au events were above 24 ag for B cells exposed to 13 nm K7C-modified AuNPs. We measured a maximum ^{197}Au mass of 50 000 ag per cell, the maximum mass the SC-ICP-MS instrument could detect for these conditions. Collectively, our quantitative SC-ICP-MS results indicated that K7C-modified AuNPs enhanced B cell nanoparticle association on average ~ 100 -fold compared to mPEG-AuNPs.

We then qualitatively assessed nanoparticle association with B cells with CLSM using a label-free light scattering approach to visualize AuNPs associated with B cells.^{47,48} Due to the ability of metallic nanoparticles to scatter light, fluorophores were not required to visualize AuNPs. Interestingly, only B cells exposed to K7C-modified AuNPs had detectable intracellular CLSM light scattering signals (Figure 2C). On the other hand, B cells exposed to mPEG-modified AuNPs (Figure 2D) lacked detectable CLSM light scattering signals, similar to B cells without AuNPs (Figures 2E). These qualitative label-free CLSM-based imaging results corroborated

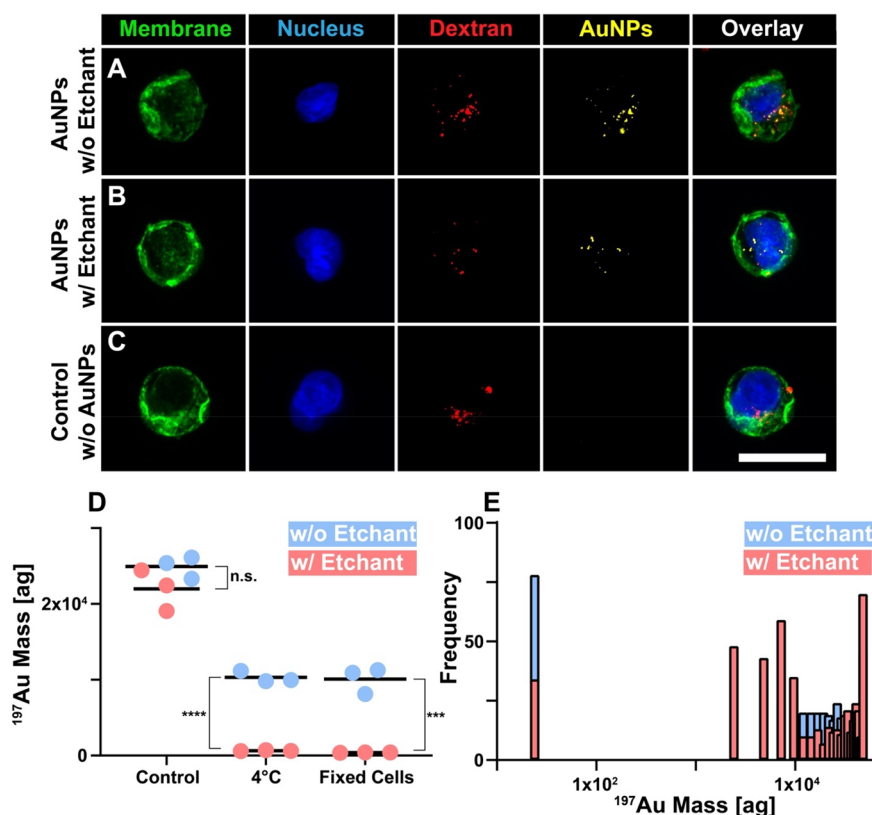


Figure 3. Visualizing and quantifying nanoparticle interactions with individual B cells. (A–C) Confocal laser scanning microscopy (CLSM) maximum intensity projections (MIP) of B cells exposed to 13 nm AuNPs surface-modified with K7C peptides for 8 h without (A) and with (B) exposure to KI/I₂ etchant that dissolves AuNPs. (C) CLSM maximum intensity projection (MIP) images of B cells without AuNPs exposure (cell only control group). Scale bar represents 20 μm . The intracellular vesicles were labeled with fluorescently tagged dextran. (D) Average ^{197}Au masses of individual B cells exposed to 13 nm AuNPs surface-modified with K7C peptides under different conditions for 8 h without etchant (blue) and with an etchant (red). Circles represent the average ^{197}Au mass of ≥ 500 ^{197}Au events. Bars represent the averages of three independent measurements. Unpaired T-Test was used to determine the statistical significance between the average ^{197}Au mass before and after etching (n.s. = no significance; *** $p \leq 0.001$, **** $p \leq 0.0001$). (E) The ^{197}Au mass distribution based on individual B cells exposed to 13 nm AuNPs surface-modified with K7C peptides without etchant (blue) and with an etchant (red).

the SP-ICP-MS results and demonstrated how nanoparticle surface charge governed nanoparticle interactions with individual B cells. To assess the biocompatibility of the K7C-modified AuNPs, we evaluated the viability of B cells exposed to several different concentrations of K7C-modified AuNPs with a colorimetric viability assay (Figure S12). The assay confirmed that our cationic peptide-modified AuNPs were a safe model for further investigating nanoparticle–cell interactions at the single B cell level.

Previous studies used KI/I₂ etching to remove extracellular AuNPs in cell culture experiments.⁴⁵ We wondered whether this approach could be adopted for quantifying internalized vs associated AuNPs at the single B cell level. We confirmed that, upon exposure to KI/I₂ etchant solution, 13 nm AuNPs were undetectable by dynamic light scattering (DLS) and no longer exhibited the characteristic surface plasmon resonance-based absorption properties using UV–vis spectrophotometry, thus indicating the dissolution of the AuNPs (Table S4 and Figure S13). To visualize nanoparticle uptake within B cells, we first examined B cells exposed to AuNPs with and without KI/I₂ etchant using CLSM. To help identify internalized AuNPs, we tracked intracellular vesicles with fluorescently modified dextran and acquired CLSM Z-stacks of B cells exposed to 13 nm K7C peptide-modified AuNPs (Figure 3A).⁵⁰ The representative Z-projection in Figure 3A shows colocalization

between AuNP scattering signal and fluorescently labeled intracellular vesicles. Upon exposing B cells to KI/I₂ etchant, the nanoparticles were still localized within intracellular vesicles (Figures 3B). Our CLSM images indicated that B cells internalized nanoparticles within intracellular vesicles and that these internalized nanoparticles did not degrade upon KI/I₂ etchant exposure.

We then used SC-ICP-MS to quantify the number of internalized AuNPs per individual B cell. We first obtained the average ^{197}Au mass of B cells exposed to 13 nm K7C peptide-modified AuNPs with and without KI/I₂ etchant treatment (Figure 3D). The average ^{197}Au mass decreased by ~ 3000 ag after the B cells were exposed to KI/I₂ etchant, indicating that only ~ 125 AuNPs had been etched away. These results were validated by CLSM imaging and suggested that K7C peptide-modified AuNPs were engulfed by cells instead of adhering to the B cell membrane. To confirm the KI/I₂ etchant's ability to remove surface-bound AuNPs, we exposed B cells to K7C peptide-modified AuNPs at 4 $^{\circ}\text{C}$. This temperature reduces a cell's membrane fluidity and effectively inhibits nanoparticle endocytosis.⁴⁶ We observed that the B cells kept at 4 $^{\circ}\text{C}$ exhibited an average of $\sim 10\,000$ ag of associated ^{197}Au corresponding to ~ 417 AuNPs per cell. However, after the cells were exposed to the KI/I₂ etchant, the number of ^{197}Au

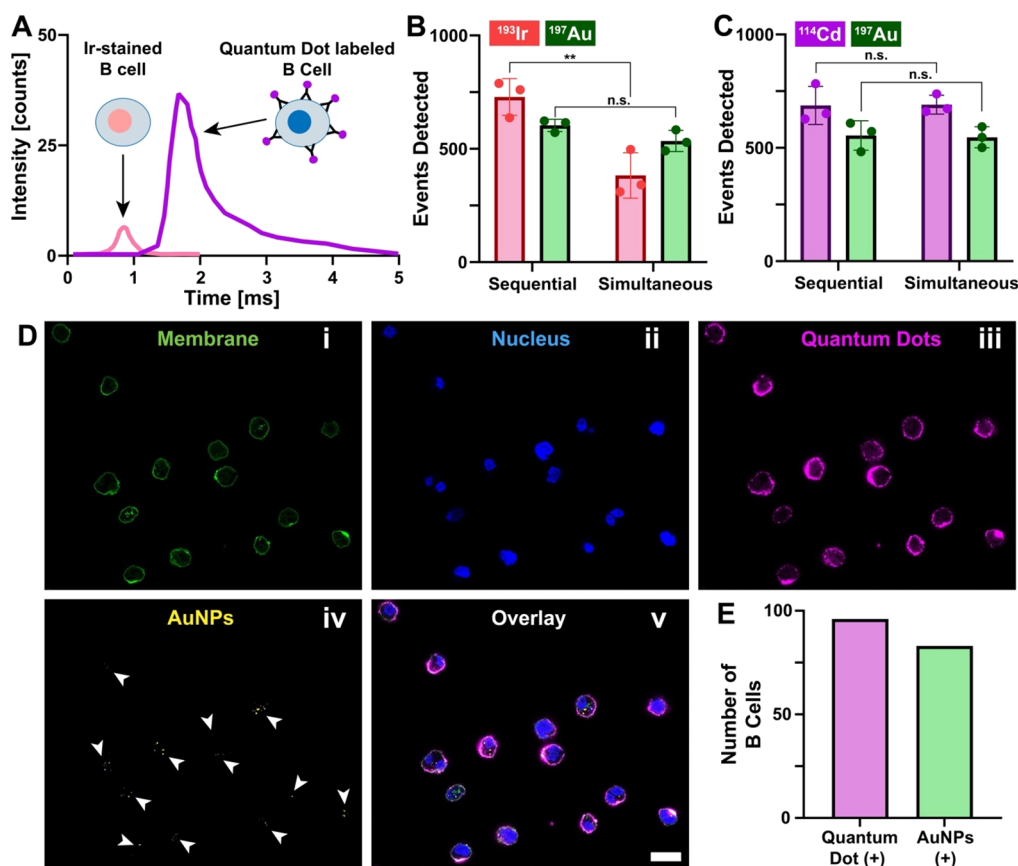


Figure 4. Determining AuNP⁺ B cells with dual-analyte SC-ICP-MS. (A) Transient ion peak shapes of cadmium and iridium labeled B cells using optimized dual-analyte SC-ICP-MS conditions to detect ^{193}Ir and ^{114}Cd . (B) SC-ICP-MS determination of AuNP⁺ B cells with sequential and simultaneous analysis of ^{193}Ir and ^{197}Au in individual B cells exposed to 13 nm AuNPs surface-modified with K7C peptides for 8 h. Bars represent mean values with standard deviations from three independent measurements. (C) SC-ICP-MS determination of AuNP⁺ B cells with sequential and simultaneous analysis of ^{114}Cd and ^{197}Au in individual B cells exposed to 13 nm AuNPs surface-modified with K7C peptides for 8 h. Bars represent mean values with standard deviations from three independent measurements. Unpaired T-Test was used to determine the statistical significance between events detected with sequential measurements or simultaneous measurements of cell markers and AuNPs (n.s. = no significance; ** $p \leq 0.01$). (D) Representative confocal laser scanning microscopy (CLSM) images of B cells exposed to 13 nm AuNPs surface-modified with K7C peptides for 8 h and labeled with streptavidin-coated quantum dots via biotinylated anti-CD19 antibodies. Images i–v display different emission channels. Scale bar represents 20 μm . (E) The number of quantum dot labeled B cells (quantum dot⁺ and AuNPs⁺ cells). The numbers were obtained using representative CLSM images (40x objective) with AuNP scattering intensity from multiple fields of view.

events decreased and over 9000 ag of ^{197}Au (~ 375 AuNPs) were removed per B cell (Figure 3C).

Similarly, B cells that were fixed with 4% paraformaldehyde before exposure to K7C peptide-modified AuNPs exhibited an average of $\sim 10\,000$ ag of associated ^{197}Au per individual B cell. Upon KI/I₂ etchant exposure, these fixed B cells lost over 9000 ag of ^{197}Au per individual B cell. Our SC-ICP-MS data showed that although K7C peptide-modified AuNPs efficiently associated with B cells, approximately 95% of extracellular AuNPs could be removed upon chemical etching. These results were further corroborated by the mass distribution of single B cells before and after KI/I₂ etching (Figure 3E). Our KI/I₂ etching results revealed that K7C peptide-modified AuNPs accumulated inside B cells through energy-dependent mechanisms, likely endocytosis, which we quantified at the single cell level with SC-ICP-MS.

Since quadrupole SC-ICP-MS is limited to detecting one element per cell event, cells without AuNPs were not detected. To overcome this limitation, we sought to simultaneously analyze a cell marker and AuNPs using our previously established dual analyte quadrupole ICP-MS technique.²³ Briefly, transient ion signals of analytes are elongated, allowing

the quadrupole mass filter to switch between two different isotopes per event efficiently. First, we compared transient ion signals of iridium-stained B cells and quantum dot labeled B cells under conditions that enable the simultaneous detection of two isotopes per event on quadrupole ICP-MS (Table S5). Figure 4A shows that the transient ion cloud for quantum dot labeled B cells extends up to 5 ms with a maximum intensity of ~ 35 counts, whereas the iridium-stained B cells had 5-fold fewer counts and barely lasted 2 ms (Figure 4A). B cells exposed to K7C peptide-modified AuNPs exhibited transient ^{197}Au signal durations >5 ms with intensities over 100 counts under optimized dual analyte ICP-MS conditions (Figure S14). These millisecond transient ion signals pointed to the possibility of efficient quadrupole mass filter switching between a cell marker and internalized AuNPs, thus enabling the simultaneous detection of B cells that were positive or negative for AuNPs using quadrupole ICP-MS. We found that only quantum dot labeled B cells enabled the accurate simultaneous determination of individual B cells that had internalized AuNPs in dual analyte SC-ICP-MS mode (Figure 4B). When ^{114}Cd and ^{197}Au were measured sequentially (i.e., one isotope at a time) $81.1 \pm 8.9\%$ of B cells were positive for AuNPs (i.e.,

AuNP⁺). Similarly, when ¹¹⁴Cd and ¹⁹⁷Au were measured simultaneously (i.e., both isotopes detected simultaneously under optimized dual analyte SC-ICP-MS conditions), 79.6 ± 11.1% of B cells were AuNP⁺. We only found similar results when ¹⁹³Ir and ¹⁹⁷Au were measured sequentially (83.2 ± 6.1%, Figure 4C). However, when ¹⁹³Ir and ¹⁹⁷Au were measured simultaneously, the number of ¹⁹³Ir events decreased by ~50% (Figure 4C). These results indicated that although iridium staining of individual B cells worked well for the detection of single cells in single analyte mode on quadrupole-based SC-ICP-MS, the high signal intensity and long millisecond transient ion signals from quantum dot nanoparticles and AuNPs were needed for the accurate simultaneous measurement of two different analytes in a single cell.

We corroborated our dual analyte SC-ICP-MS results with CLSM imaging and showed that B cells labeled with quantum dots and exposed to K7C peptide-modified AuNPs could be visualized (Figure 4D). To provide a better understanding of how many B cells had AuNPs, we counted 96 representative quantum dot-labeled B cells from multiple fields of view and determined that 83 of those cells exhibited AuNP scattering intensity, indicating that ~87% of B cells had internalized AuNPs (Figure 4E).

In conclusion, we showed that human B cells labeled with either an intracellular (DNA) stain (iridium) or surface-bound labels (quantum dots) enabled the detection and quantification of individual B cells using quadrupole SC-ICP-MS at a maximum rate of ~30 cells per second. We quantified the AuNP association with B cells at the single cell level and observed that positively charged AuNPs safely enhanced B cell association ~100-fold compared to neutral AuNPs. We further demonstrated the ability to quantify internalized AuNPs with SC-ICP-MS and showed that these nanoparticles entered B cells through active internalization pathways. Lastly, we determined that >80% of B cells had internalized AuNPs by using quantum dot labeling in combination with a quantitative dual analyte SC-ICP-MS workflow and corroborated the findings with label-free light scattering-based CLSM imaging. The demonstrated SC-ICP-MS workflow could potentially be adopted and expanded to quantify nanoparticle–cell interactions with organic nanoparticles bearing metal tags. Our established SC-ICP-MS workflow provides a quantitative framework for researchers who seek to understand nanoparticle–cell interactions at the single cell level with far-reaching implications for nano ecology, nanotoxicology, and nanomedicine, including nanovaccines.

■ ASSOCIATED CONTENT

SI Supporting Information

The Supporting Information is available free of charge at <https://pubs.acs.org/doi/10.1021/acs.nanolett.2c01037>.

Additional Equation S1, Figures S1–S14, Tables S1–S5, and methods and materials. (PDF)

■ AUTHOR INFORMATION

Corresponding Author

Stefan Wilhelm – Stephenson School of Biomedical Engineering, University of Oklahoma, Norman, Oklahoma 73019, United States; Institute for Biomedical Engineering, Science, and Technology (IBEST), Norman, Oklahoma 73019, United States; Stephenson Cancer Center, Oklahoma

City, Oklahoma 73104, United States; orcid.org/0000-0003-2167-6221; Email: stefan.wilhelm@ou.edu

Authors

Nathan D. Donahue – Stephenson School of Biomedical Engineering, University of Oklahoma, Norman, Oklahoma 73019, United States

Vinit Sheth – Stephenson School of Biomedical Engineering, University of Oklahoma, Norman, Oklahoma 73019, United States

Alex N. Frickenstein – Stephenson School of Biomedical Engineering, University of Oklahoma, Norman, Oklahoma 73019, United States

Alyssa Holden – Stephenson School of Biomedical Engineering, University of Oklahoma, Norman, Oklahoma 73019, United States

Sandy Kanapilly – PerkinElmer, Waltham, Massachusetts 02451, United States

Chady Stephan – PerkinElmer, Woodbridge, ON L4L8H1, Canada

Complete contact information is available at:

<https://pubs.acs.org/10.1021/acs.nanolett.2c01037>

Notes

The authors declare no competing financial interest.

■ ACKNOWLEDGMENTS

The authors acknowledge the assistance of Drs. S. Foster, P. Larson, J. Sabisch, S. Liang, B. Fowler, and J. Willige. Additionally, the authors acknowledge the University of Oklahoma (OU) Samuel Roberts Noble Microscopy Laboratory (SRNML), the OU Mass Spectrometry, Proteomics & Metabolomics (MSPM) Core, and the Oklahoma Medical Research Foundation (OMRF) Imaging Core Facility for assistance. The authors thank Drs. Irvine and Melo for kindly providing the Raji cell line. This work was supported in part by an NSF MRI grant (1828234), NSF CAREER award (2048130), an NIH COBRE award (P20GM135009), an IBEST/OUHSC seed grant for interdisciplinary research, the OU VPRP Strategic Equipment Investment grant, the OU Faculty Investment Program, an OCAST Health Research grant (HR20-106), and the Oklahoma Tobacco Settlement Endowment Trust awarded to the University of Oklahoma - Stephenson Cancer Center. The content is solely the responsibility of the authors and does not necessarily represent the official views of the Oklahoma Tobacco Settlement Endowment Trust.

■ REFERENCES

- (1) Singh, A. Eliciting B Cell Immunity against Infectious Diseases Using Nanovaccines. *Nat. Nanotechnol.* 2020 161 2021, 16 (1), 16–24.
- (2) Kranz, L. M.; Diken, M.; Haas, H.; Kreiter, S.; Loquai, C.; Reuter, K. C.; Meng, M.; Fritz, D.; Vascotto, F.; Hefesha, H.; Grunwitz, C.; Vormehr, M.; Husemann, Y.; Selmi, A.; Kuhn, A. N.; Buck, J.; Derhovanessian, E.; Rae, R.; Attig, S.; Diekmann, J.; Jabulowsky, R. A.; Heesch, S.; Hassel, J.; Langguth, P.; Grabbe, S.; Huber, C.; Türeci, Ö.; Sahin, U. Systemic RNA Delivery to Dendritic Cells Exploits Antiviral Defence for Cancer Immunotherapy. *Nature* 2016, 534 (7607), 396–401.
- (3) Zilker, C.; Kozlova, D.; Sokolova, V.; Yan, H.; Epple, M.; Überla, K.; Temchura, V. Nanoparticle-Based B-Cell Targeting Vaccines: Tailoring of Humoral Immune Responses by Functionalization with

- Different TLR-Ligands. *Nanomedicine Nanotechnology, Biol. Med.* **2017**, *13* (1), 173–182.
- (4) Irvine, D. J.; Read, B. J. Shaping Humoral Immunity to Vaccines through Antigen-Displaying Nanoparticles. *Curr. Opin. Immunol.* **2020**, *65*, 1–6.
- (5) Kurosaki, T.; Kometani, K.; Ise, W. Memory B Cells. *Nat. Rev. Immunol.* **2015**, *15* (3), 149–159.
- (6) Inoue, T.; Moran, I.; Shinnakasu, R.; Phan, T. G.; Kurosaki, T. Generation of Memory B Cells and Their Reactivation. *Immunol. Rev.* **2018**, *283* (1), 138–149.
- (7) Tsoi, K. M.; Macparland, S. A.; Ma, X. Z.; Spetzler, V. N.; Echeverri, J.; Ouyang, B.; Fadel, S. M.; Sykes, E. A.; Goldaracena, N.; Kathis, J. M.; Conneely, J. B.; Alman, B. A.; Selzner, M.; Ostrowski, M. A.; Adeyi, O. A.; Zilman, A.; McGilvray, I. D.; Chan, W. C. W. Mechanism of Hard-Nanomaterial Clearance by the Liver. *Nat. Mater.* **2016**, *15* (11), 1212–1221.
- (8) Almeida, J. P. M.; Lin, A. Y.; Langsner, R. J.; Eckels, P.; Foster, A. E.; Drezek, R. A. In Vivo Immune Cell Distribution of Gold Nanoparticles in Naïve and Tumor Bearing Mice. *Small* **2014**, *10* (4), 812–819.
- (9) Martin, J. T.; Cottrell, C. A.; Antanasijevic, A.; Carnathan, D. G.; Cossette, B. J.; Enemu, C. A.; Gebru, E. H.; Choe, Y.; Viviano, F.; Fischinger, S.; Tokatlian, T.; Cirelli, K. M.; Ueda, G.; Copps, J.; Schiffner, T.; Menis, S.; Alter, G.; Schief, W. R.; Crotty, S.; King, N. P.; Baker, D.; Silvestri, G.; Ward, A. B.; Irvine, D. J. Targeting HIV Env Immunogens to B Cell Follicles in Nonhuman Primates through Immune Complex or Protein Nanoparticle Formulations. *npj Vaccines* **2020**, *5* (1). DOI: 10.1038/s41541-020-00223-1.
- (10) Kato, Y.; Abbott, R. K.; Freeman, B. L.; Haupt, S.; Groschel, B.; Silva, M.; Menis, S.; Irvine, D. J.; Schief, W. R.; Crotty, S. Multifaceted Effects of Antigen Valency on B Cell Response Composition and Differentiation In Vivo. *Immunity* **2020**, *53* (3), 548–563 e8.
- (11) Yang, W.; Wang, L.; Mettenbrink, E. M.; Deangelis, P. L.; Wilhelm, S. Nanoparticle Toxicology. *Annu. Rev. Pharmacol. Toxicol.* **2021**, *61*, 269–289.
- (12) Narum, S. M.; Le, T.; Le, D. P.; Lee, J. C.; Donahue, N. D.; Yang, W.; Wilhelm, S. Passive Targeting in Nanomedicine: Fundamental Concepts, Body Interactions, and Clinical Potential. In *Nanoparticles for Biomedical Applications*; Elsevier: 2020; pp 37–53. DOI: 10.1016/b978-0-12-816662-8.00004-7.
- (13) Gottstein, C.; Wu, G.; Wong, B. J.; Zasadzinski, J. A. Precise Quantification of Nanoparticle Internalization. *ACS Nano* **2013**, *7* (6), 4933–4945.
- (14) Shin, H.; Kwak, M.; Lee, T. G.; Lee, J. Y. Quantifying the Level of Nanoparticle Uptake in Mammalian Cells Using Flow Cytometry. *Nanoscale* **2020**, *12* (29), 15743–15751.
- (15) Wu, Y.; Ali, M. R. K.; Dansby, K.; El-Sayed, M. A. Improving the Flow Cytometry-Based Detection of the Cellular Uptake of Gold Nanoparticles. *Anal. Chem.* **2019**, *91*, 14261.
- (16) Romeu, H. G.; Deville, S.; Salvati, A. Time- and Space-Resolved Flow-Cytometry of Cell Organelles to Quantify Nanoparticle Uptake and Intracellular Trafficking by Cells. *Small* **2021**, *17* (34), 2100887.
- (17) Zucker, R. M.; Massaro, E. J.; Sanders, K. M.; Degn, L. L.; Boyes, W. K. Detection of TiO₂ Nanoparticles in Cells by Flow Cytometry. *Cytom. Part A* **2010**, *77A* (7), 677–685.
- (18) Elsaesser, A.; Taylor, A.; Yanés, G. S. de; McKerr, G.; Kim, E.-M.; O'Hare, E.; Howard, C. V. Quantification of Nanoparticle Uptake by Cells Using Microscopical and Analytical Techniques. <https://doi.org/10.2217/nmm.10.118> **2010**, *5* (9), 1447–1457.
- (19) Suutari, T.; Silen, T.; Karaman, D. S.; Saari, H.; Desai, D.; Kerkelä, E.; Laitinen, S.; Hanzlikova, M.; Rosenholm, J. M.; Yliperttula, M.; Viitala, T. Real-Time Label-Free Monitoring of Nanoparticle Cell Uptake. *Small* **2016**, *12* (45), 6289–6300.
- (20) Yang, Y. S. S.; Atukorale, P. U.; Moynihan, K. D.; Bekdemir, A.; Rakhra, K.; Tang, L.; Stellacci, F.; Irvine, D. J. High-Throughput Quantitation of Inorganic Nanoparticle Biodistribution at the Single-Cell Level Using Mass Cytometry. *Nat. Commun.* **2017**, *8* (1), 1–11.
- (21) Malysheva, A.; Ivask, A.; Doolette, C. L.; Voelcker, N. H.; Lombi, E. Cellular Binding, Uptake and Biotransformation of Silver Nanoparticles in Human T Lymphocytes. *Nat. Nanotechnol.* **2021**, *16* (8), 926–932.
- (22) Pichaandi, J.; Tong, L.; Bouzekri, A.; Yu, Q.; Ornatsky, O.; Baranov, V.; Winnik, M. A. Liposome-Encapsulated NaLnF₄ Nanoparticles for Mass Cytometry: Evaluating Nonspecific Binding to Cells. *Chem. Mater.* **2017**, *29*, 4980–4990.
- (23) Donahue, N. D.; Kanapilly, S.; Stephan, C.; Marlin, M. C.; Francek, E. R.; Haddad, M.; Guthridge, J.; Wilhelm, S. Quantifying Chemical Composition and Reaction Kinetics of Individual Colloidally Dispersed Nanoparticles. *Nano Lett.* **2022**, *22* (1), 294–301.
- (24) Merrifield, R. C.; Stephan, C.; Lead, J. R. Quantification of Au Nanoparticle Biouptake and Distribution to Freshwater Algae Using Single Cell - ICP-MS. *Environ. Sci. Technol.* **2018**, *52* (4), 2271–2277.
- (25) Gomez-Gomez, B.; Corte-Rodríguez, M.; Perez-Corona, M. T.; Bettmer, J.; Montes-Bayón, M.; Madrid, Y. Combined Single Cell and Single Particle ICP-TQ-MS Analysis to Quantitatively Evaluate the Uptake and Biotransformation of Tellurium Nanoparticles in Bacteria. *Anal. Chim. Acta* **2020**, *1128*, 116–128.
- (26) Álvarez-Fernández García, R.; Corte-Rodríguez, M.; Macke, M.; Leblanc, K. L.; Mester, Z.; Montes-Bayón, M.; Bettmer, J. Addressing the Presence of Biogenic Selenium Nanoparticles in Yeast Cells: Analytical Strategies Based on ICP-TQ-MS. *Analyst* **2020**, *145* (4), 1457–1465.
- (27) Rasmussen, L.; Shi, H.; Liu, W.; Shannon, K. B. Quantification of Silver Nanoparticle Interactions with Yeast *Saccharomyces Cerevisiae* Studied Using Single-Cell ICP-MS. *Anal. Bioanal. Chem.* **2022**, *414*, 3077.
- (28) Corte Rodríguez, M.; Álvarez-Fernández García, R.; Blanco, E.; Bettmer, J.; Montes-Bayón, M. Quantitative Evaluation of Cisplatin Uptake in Sensitive and Resistant Individual Cells by Single-Cell ICP-MS (SC-ICP-MS). *Anal. Chem.* **2017**, *89* (21), 11491–11497.
- (29) Cao, Y.; Feng, J.; Tang, L.; Yu, C.; Mo, G.; Deng, B. A Highly Efficient Introduction System for Single Cell- ICP-MS and Its Application to Detection of Copper in Single Human Red Blood Cells. *Talanta* **2020**, *206* (July 2019), 120174.
- (30) Chun, K. H.; Lum, J. T. S.; Leung, K. S. Y. Dual-Elemental Analysis of Single Particles Using Quadrupole-Based Inductively Coupled Plasma-Mass Spectrometry. *Anal. Chim. Acta* **2022**, *1192*, 339389.
- (31) Wilhelm, S.; Bensen, R. C.; Kothapali, N. R.; et al. Quantification of gold nanoparticle uptake into cancer cells using single cell ICPMS. *PerkinElmer Appl. Note* **2018**, 1–4.
- (32) Yin, L.; Zhang, Z.; Liu, Y.; Gao, Y.; Gu, J. Recent Advances in Single-Cell Analysis by Mass Spectrometry. *Analyst* **2019**, *144* (3), 824–845.
- (33) Fousek, K.; Watanabe, J.; Joseph, S. K.; George, A.; An, X.; Byrd, T. T.; Morris, J. S.; Luong, A.; Martínez-Paniagua, M. A.; Sanber, K.; Navai, S. A.; Gad, A. Z.; Salsman, V. S.; Mathew, P. R.; Kim, H. N.; Wagner, D. L.; Brunetti, L.; Jang, A.; Baker, M. L.; Varadarajan, N.; Hegde, M.; Kim, Y.-M.; Heisterkamp, N.; Abdel-Aziz, H.; Ahmed, N. CAR T-Cells That Target Acute B-Lineage Leukemia Irrespective of CD19 Expression. *Leuk.* **2020**, *351* **2021**, *35* (1), 75–89.
- (34) Webster, B.; Xiong, Y.; Hu, P.; Wu, D.; Alabanza, L.; Orentas, R. J.; Drolpic, B.; Schneider, D. Self-Driving Armored CAR-T Cells Overcome a Suppressive Milieu and Eradicate CD19+ Raji Lymphoma in Preclinical Models. *Mol. Ther.* **2021**, *29* (9), 2691–2706.
- (35) Bjornson, Z. B.; Nolan, G. P.; Fantl, W. J. Single Cell Mass Cytometry for Analysis of Immune System Functional States. *Curr. Opin. Immunol.* **2013**, *25* (4), 484–494.
- (36) Ijsselstein, M. E.; van der Breggen, R.; Farina Sarasqueta, A.; Koning, F.; de Miranda, N. F. C. C. A 40-Marker Panel for High Dimensional Characterization of Cancer Immune Microenvironments by Imaging Mass Cytometry. *Front. Immunol.* **2019**, *10* (OCT), 2534.
- (37) Donahue, N. D.; Francek, E. R.; Kiyotake, E.; Thomas, E. E.; Yang, W.; Wang, L.; Detamore, M. S.; Wilhelm, S. Assessing Nanoparticle Colloidal Stability with Single-Particle Inductively

Coupled Plasma Mass Spectrometry (SP-ICP-MS). *Anal. Bioanal. Chem.* **2020**, *412* (22), 5205–5216.

(38) Corte-Rodríguez, M.; Álvarez-Fernández, R.; García-Cancela, P.; Montes-Bayón, M.; Bettmer, J. Single Cell ICP-MS Using on Line Sample Introduction Systems: Current Developments and Remaining Challenges. *TrAC Trends Anal. Chem.* **2020**, *132*, 116042.

(39) Theiner, S.; Loehr, K.; Koellensperger, G.; Mueller, L.; Jakubowski, N. Single-Cell Analysis by Use of ICP-MS. *J. Anal. At. Spectrom.* **2020**, *35* (9), 1784–1813.

(40) Lum, J. T. S.; Leung, K. S. Y. Quantifying Silver Nanoparticle Association and Elemental Content in Single Cells Using Dual Mass Mode in Quadrupole-Based Inductively Coupled Plasma-Mass Spectrometry. *Anal. Chim. Acta* **2019**, *1061*, 50–59.

(41) Wang, H.; Wang, B.; Wang, M.; Zheng, L.; Chen, H.; Chai, Z.; Zhao, Y.; Feng, W. Time-Resolved ICP-MS Analysis of Mineral Element Contents and Distribution Patterns in Single Cells. *Analyst* **2015**, *140* (2), 523–531.

(42) Finck, R.; Simonds, E. F.; Jager, A.; Krishnaswamy, S.; Sachs, K.; Fantl, W.; Pe'er, D.; Nolan, G. P.; Bendall, S. C. Normalization of Mass Cytometry Data with Bead Standards. *Cytometry Part A* **2013**, *83A*, 483–494.

(43) Olesik, J. W.; Gray, P. J. Considerations for Measurement of Individual Nanoparticles or Microparticles by ICP-MS: Determination of the Number of Particles and the Analyte Mass in Each Particle. *J. Anal. At. Spectrom.* **2012**, *27* (7), 1143–1155.

(44) Perrault, S.; Chan, W. Synthesis and Surface Modification of Highly Monodispersed, Spherical Gold Nanoparticles of 50–200 Nm. *J. Am. Chem. Soc.* **2009**, *131* (47), 17042–17043.

(45) Lee, J. C.; Donahue, N. D.; Mao, A. S.; Karim, A.; Komarneni, M.; Thomas, E. E.; Francek, E. R.; Yang, W.; Wilhelm, S. Exploring Maleimide-Based Nanoparticle Surface Engineering to Control Cellular Interactions. *ACS Appl. Nano Mater.* **2020**, *3*, 2421.

(46) Donahue, N. D.; Acar, H.; Wilhelm, S. Concepts of Nanoparticle Cellular Uptake, Intracellular Trafficking, and Kinetics in Nanomedicine. *Adv. Drug Delivery Rev.* **2019**, *143*, 68.

(47) Wang, F.; Chen, B.; Yan, B.; Yin, Y.; Hu, L.; Liang, Y.; Song, M.; Jiang, G. Scattered Light Imaging Enables Real-Time Monitoring of Label-Free Nanoparticles and Fluorescent Biomolecules in Live Cells. *J. Am. Chem. Soc.* **2019**, *141* (36), 14043–14047.

(48) Yang, W.; Wang, L.; Fang, M.; Sheth, V.; Zhang, Y.; Holden, A. M.; Donahue, N. D.; Green, D. E.; Frickenstein, A. N.; Mettenbrink, E. M.; Schwemley, T. A.; Francek, E. R.; Haddad, M.; Hossen, M. N.; Mukherjee, S.; Wu, S.; DeAngelis, P. L.; Wilhelm, S. Nanoparticle Surface Engineering with Heparosan Polysaccharide Reduces Serum Protein Adsorption and Enhances Cellular Uptake. *Nano Lett.* **2022**, *22* (5), 2103–2111.

(49) Cho, E. C.; Xie, J.; Wurm, P. A.; Xia, Y. Understanding the Role of Surface Charges in Cellular Adsorption versus Internalization by Selectively Removing Gold Nanoparticles on the Cell Surface with a I 2/KI Etchant. *Nano Lett.* **2009**, *9* (3), 1080–1084.

(50) Sheth, V.; Wang, L.; Bhattacharya, R.; Mukherjee, P.; Wilhelm, S. Strategies for Delivering Nanoparticles across Tumor Blood Vessels. *Adv. Funct. Mater.* **2021**, *31* (8), 2007363.